Ruthenium Nitrosyl Porphyrins Coordinated with Aryloxides Containing Internal Hydrogen Bonds

Adam J. Warhausen,*[a] Jeremy R. Zink,[b] Bradley J. Ross,[a,b] Anthony R. Ramuglia,[c] Jennifer Londoño-Salazar,[b] Michael J. Shaw,[c] and George B. Richter-Addo*[b]

[a] Dr. Adam J. Warhausen, Bradley J. Ross
Department of Chemistry
Saginaw Valley State University
7400 Bay Road, University Center, MI 4871, USA
E-mail: awarhaus@svsu.edu, bjross1@svsu.edu

[b] Dr. Jeremy R. Zink, Dr. Jennifer Londoño-Salazar, Dr. George B. Richter-Addo
Department of Chemistry and Biochemistry
University of Oklahoma
101 Stephenson Parkway, Norman, OK 73019, USA
Email: jzink273@gmail.com, Jennifer.londono@ou.edu, grichteraddo@ou.edu

[b] Anthony R. Ramuglia, Dr. Michael J. Shaw
Department of Chemistry
Southern Illinois University Edwardsville
Edwardsville, IL 62025, USA
Email: Anthony.ramuglia@tu-dresden.de, michsha@siue.edu

Supporting information for this article is given via a link at the end of the document.

Abstract: The synthesis, characterization, and redox behavior of aryloxide complexes containing an increasing number of internal hydrogen bonds (OEP)Ru(NO)(OAr_{xH}) (OEP = octaethylporphyrinato dianion; x = 0, 1, 2) are reported. These nitrosyl aryloxide compounds were characterized by X-ray crystallography, IR and ^{1}H NMR spectroscopy. The IR spectra displayed υ_{NO} frequencies in the 1823–1843 cm^{-1} range with compounds possessing more internal hydrogen bonds demonstrating higher υ_{NO} frequencies due to diminished π-backdonation to the Ru-NO fragment. Comparison of the distinct υ_{NH} and δ_{N-H} signals in the IR and ^{1}H NMR spectra of the free and complexed OAr_{1H}/OAr_{2H} ligands support the notion of additional electron density being removed via intramolecular hydrogen bonding. Results of DFT calculations on the (porphine)Ru(NO)(OAr_{xH}) models (porphine = unsubstituted porphyrin) reveal that the HOMOs of these complexes have significant axial ligand contributions, whereas the HOMOs of the five-coordinate [(porphine)RuNO)]$^+$ cation resides mostly on the equatorial porphyrin macrocycle. The electrochemical results of these (OEP)Ru(NO)(OAr_{xH}) complexes in CH_2Cl_2 reveal first oxidations that occur at increasingly positive potentials when more internal hydrogen bonds are present. Based on the DFT and preliminary IR spectroelectrochemical results, we propose that the electrooxidations result in eventual dissociation of the axial aryloxide ligands.

Introduction

The proximal tyrosinate ligand in heme catalase displays H-bonding interactions with a nearby Arg residue.[1-5] Such H-bonding interactions with the proximal ligands of heme proteins are not uncommon, and these secondary interactions help modulate the electron-donating properties of the proximal ligands and hence the redox behaviors of the heme cofactors. Classic examples include studies of these effects in cysteinate-ligated hemes (e.g., cytochrome P450 and NO synthase) and other tyrosinate-ligated hemes (e.g., HTHP, mauG, cAOS, IsdB).[6-9] The interactions of NO with metalloporphyrins and heme have also been reviewed.[10-11]

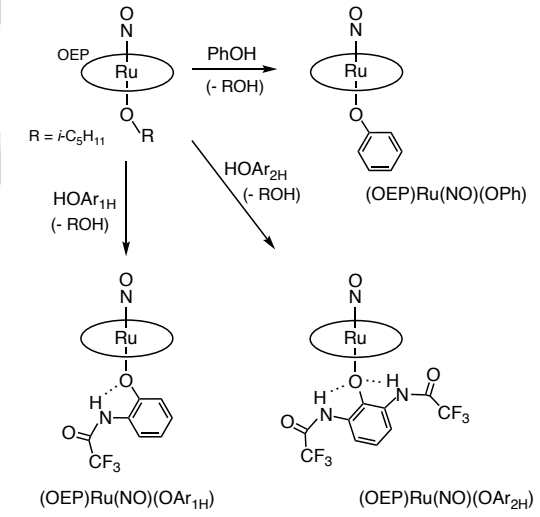

Figure 1. Synthesis of the (OEP)Ru(NO)(OAr_{xH}) complexes.

Chemical modeling of heme cofactors has frequently employed the second-row transition metal ruthenium (Ru) to limit available spin states to low-spin and to enhance kinetic stability of the isolated complexes. While studies of (por)Ru (por = porphyrinato dianion) systems have been reported by us[12-22] and others,[23-26] there are no reports to date describing the effects of

such internal H-bonding on the spectral and redox properties of such Ru derivatives. The preparation, spectral properties, crystal structures, and preliminary redox behavior for a series of (OEP)Ru(NO)(OArxH) compounds (Figure 1; OEP = octaethylpophyrinato dianion) are reported herein. The results delineate the subtle effects of these secondary H-bonding effects on the redox behavior of these compounds.

Results and Discussion

Synthesis

A series of (OEP)Ru(NO)(OAr_{xH}) compounds bearing an increasing number of intramolecular H-bonds (x = 0, 1 and 2) on the axial phenolate moiety were prepared by an alcohol exchange reaction of the precursor alkoxides (OEP)Ru(NO)(O-*i*-C_5H_{11}) with the corresponding phenol ligands. Progress of the alcohol exchange reaction was monitored by solution IR spectroscopy and considered complete when the υ_{NO} of the (OEP)Ru(NO)(O-*i*-C_5H_{11}) starting material in CH_2Cl_2 at 1792 cm^{-1} was no longer present. The utilization of this synthetic approach and specific work-up routine yielded the (OEP)Ru(NO)(OAr_{xH}) products in 61-76% yields. These target compounds are air stable as solids at room temperature and show no signs of decomposition over several weeks as determined by IR and ^{1}H NMR spectroscopy.

The distinctive υ_{NO}, υ_{CO} and υ_{NH} bands for the target nitrosyl aryloxide complexes shown in Figure 2. An exchange of the initial axial alkoxide ligands with the aryloxides resulted in a υ_{NO} shift to higher frequencies (e.g., $\Delta\upsilon_{NO}$ ~30 cm^{-1} for the OPh derivative; Figure 2a) due to the relatively electron withdrawing nature of the aryloxide group, and diminished π-backbonding of electron density to the Ru–NO moiety.

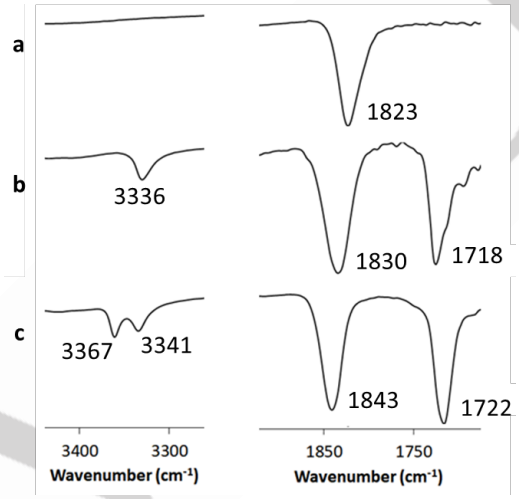

Figure 2. Truncated IR spectra of (OEP)Ru(NO)(OAr_{xH}) as KBr pellets; (a) (OEP)Ru(NO)(OPh), (b) (OEP)Ru(NO)(OAr_{1H}), (c) (OEP)Ru(NO)(OAr_{2H}), with ν_{NH} (left) and $\nu_{NO/CO}$ (right) bands labelled.

These υ_{NO} shifts are enhanced in systems containing more internal H-bonds in the axial aryloxide ligands [OAr_{2H} (1843 cm^{-1}) > OAr_{1H} (1830 cm^{-1}) > (OEP)Ru(NO)(OPh) (1823 cm^{-1})] and is a result of the presence of the internal H-bond(s) rendering the coordinating O-atoms of the aryloxides less electron-donating. In turn, less electron density on the Ru center is expected to cause a weakening of the Ru–N(O) bond and simultaneous strengthening of the N–O bond (and higher υ_{NO}). The highest observed frequencies for υ_{NO} belong to the OAr_{2H} complex, similar in value to those of the related (T(*p*-OMe)PP)Ru(NO)(OC_6HF_4) and (por)Ru(NO)X (por = TPP (tetraphenylporphyrinato dianion), T(*p*-OMe)PP, T(*p*-Me)PP, T(*p*-CF_3)PP, T(*p*-Me)P, OEP; X = Cl, Br) compounds (υ_{NO} = 1844–1855 cm^{-1}) containing more electron withdrawing ligands.[18, 27]

An equally compelling feature to the $\Delta\upsilon_{NO}$ in confirming the coordination of the axial aryloxide ligands by IR are the shifts in υ_{NH} observed in both the OAr_{1H} and OAr_{2H} compounds but not (OEP)Ru(NO)(OPh) (left of Figure 2). Comparison of the υ_{NH} values for the free ligands $HOAr_{1H}$ and $HOAr_{2H}$ (υ_{NH} = ~3385 cm^{-1}) to the corresponding coordinated complexes reveals a shift of $\Delta\upsilon_{NH}$ = ~45 cm^{-1} for (OEP)Ru(NO)(OAr_{1H}) (υ_{NH} = 3336 cm^{-1}), and (OEP)Ru(NO)(OAr_{2H}) (υ_{NH} = 3341$_{(sym)}$ and 3367$_{(asym)}$ cm^{-1}). Not surprisingly, the characteristic υ_{CO} and υ_{NH} bands of the coordinated ligands present at 1718–1722 cm^{-1} and 3336–3367 cm^{-1} regions, respectively, are similar to those previously reported for the five-coordinate (OEP)Fe(OAr_{xH}) compounds (υ_{CO} = 1722–1728 and υ_{NH} = 3355–3379 cm^{-1}).[28] Given that the OPh ligand does not possess the additional C=O or N–H functional groups that can be easily monitored by IR spectroscopy, techniques such as ^{1}H NMR spectroscopy and X-ray crystallography were essential for verifying the identity of these derivatives.

The ^{1}H NMR spectra of the (OEP)Ru(NO)(OAr_{xH}) products confirmed the absence of the alkoxide peaks of the (OEP)Ru(NO)(O-*i*-C_5H_{11}) precursor.[15, 19-20] Characteristic peaks corresponding to the porphyrin macrocycle of the desired products are considerably downfield, while the peaks belonging to the various bound phenolate moieties are shifted upfield compared to those of the free ligands. The new proton peaks of the axial ligand in (OEP)Ru(NO)(OAr_{2H}) were found in the range 5.7–6.5 ppm, contrasted to peaks of the free $HOAr_{2H}$ between 7.1-7.6 ppm. The peaks of the phenolate and N-H protons of the (OEP)Ru(NO)(OAr_{1H}) complex are found in comparable regions to the OAr_{2H} derivative, with an additional aromatic proton peak due to the mono-substituted structure shifted significantly upfield at 0.44 ppm. Similarly, the axial ligand proton peak of the (OEP)Ru(NO)(OPh) complex are found between 5.3–5.5 ppm and at 1.09 ppm due to the lack of the hydrogen bonding substituent. The ^{1}H NMR spectra and a schematic drawing of the peak assignments are shown in the Supporting Information Figures S1-S2.

Molecular Structures

The molecular structures for the target (OEP)Ru(NO)(OAr_{xH}) complexes are shown in Figure 3. The formally {RuNO}^{6} compounds exhibit near linear ∠RuNO bond angles of 172.0(4)–179.3(4)° and Ru-N(O) bond lengths in the range of 1.732(2)–1.751(5) Å. The complexed aryloxide ligands display significant bending at the Ru–O–C linkages with ∠RuOC bond angles around 122.28(15)-124.6(4)° with Ru–O bond lengths between 1.987(4)–2.045(3) Å. Unsurprisingly, these complexes most closely match the reported aryloxide complex (T(*p*-OMe)PP)Ru(NO)(OC_6HF_4)[18] with ∠RuNO and ∠RuOC bond angles of 173.1(3)° and 127.5(2)°, as well as Ru–N(O) and Ru–O bond lengths of 1.739(3) and 2.000(3) Å, respectively. Table 1 lists selected lengths and angles for the (OEP)Ru(NO)(OAr_{xH}) products. The structural data for the target aryloxide complexes

do not differ significantly in either bond lengths or angles to those of the previously reported alkoxide precursor (OEP)Ru(NO)(O-*i*-C_5H_{11}) and similar *O*-ligand derivatives.

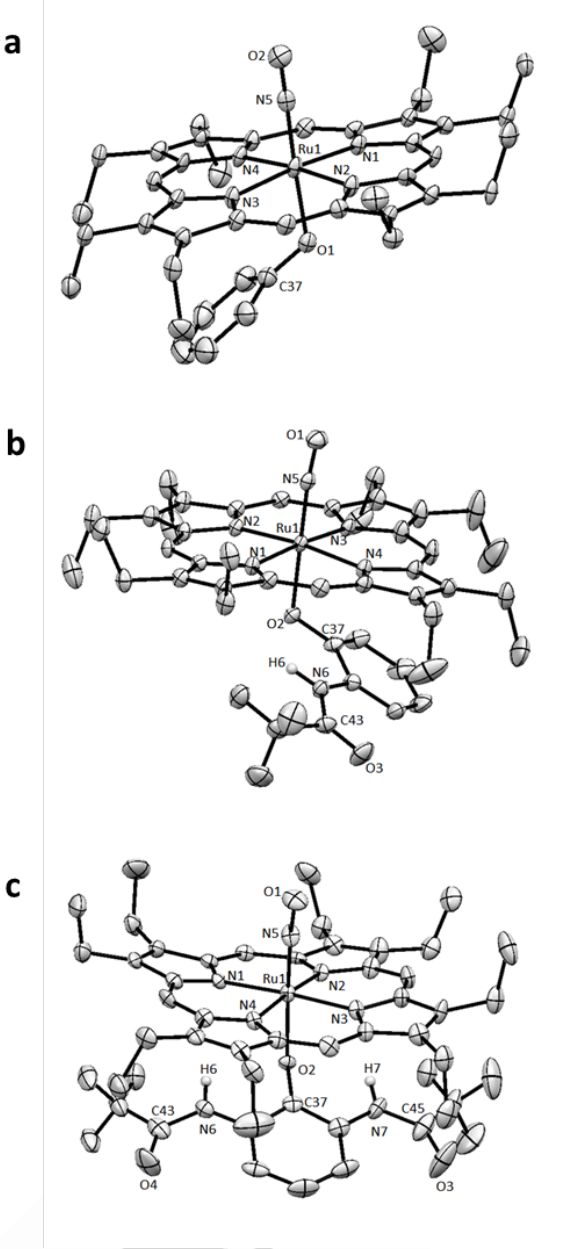

Figure 3. Crystal structures of (a) (OEP)Ru(NO)(OPh), (b) (OEP)Ru(NO)(OAr_{1H}), and (c) (OEP)Ru(NO)(OAr_{2H}). Hydrogen atoms are omitted for clarity, with the exception of the axial ligand N6-H6 and N7-H7 hydrogen atoms. Thermal ellipsoids are drawn at 50%.

The short distances between the amide H-atoms and the coordinating O-atoms (e.g., H6···O2 = 2.17 Å in the OAr_{1H} derivative) are consistent with the internal H-bonding features in the OAr_{1H} and OAr_{2H} compounds. The observed lengthening of the Ru–O bond length with increasing number of internal hydrogen bonds is similar to that reported for the five-coordinate (OEP)Fe(OAr_{xH}) compounds from Fe–OPh (1.848(4) Å) to Fe–OAr_{1H} (1.887(2) Å) to Fe–OAr_{2H} (1.926(3) Å).[28] The feature has been attributed to the removal of electron density from the coordinated oxygen via intramolecular hydrogen bonding resulting in diminished *s*-character of the coordinating O-atoms.[28]

Table 1. Selected structural data for the target (OEP)Ru(NO)(OAr_{xH}) compounds.

	OPh	OAr_{1H}	OAr_{2H}
Ru–N(O) (Å)	1.751(5)	1.732(2)	1.734(5)
Ru–O (Å)	1.987(4)	2.0296(18)	2.045(3)
Ru–N(por) (Å)	2.055(4)-2.068(4)	2.053(2)-2.059(2)	2.050(4)-2.060(4)
∠RuNO (°)	179.3(4)	174.3(2)	172.0(4)
∠RuOC (°)	124.6(4)	122.28(15)	124.5(3)

DFT Calculations

The DFT-optimized geometries of the (porphine)Ru(NO)(OAr_{xH}) compounds (not shown), where porphine is the unsubstituted porphyrinato macrocycle, reproduce the experimental OEP-containing structures quite well. We utilized these optimized structures to calculate the HOMOs and LUMOs of these compounds. The HOMOs of the model (porphine)Ru(NO)(OAr_{xH}) compounds are shown in Figure 4a-c, together with that for the five-coordinate $[(porphine)Ru(NO)]^+$ (Figure 4d). The DFT-calculated LUMOs are shown in the Supporting Information Figure S4.

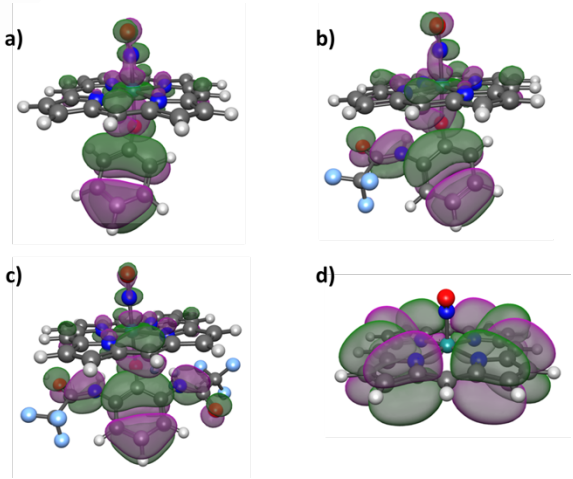

Figure 4. DFT calculated HOMOs for (a) (porphine)Ru(NO)(OPh), (b) (porphine)Ru(NO)(OAr_{1H}), (c) (porphine)Ru(NO)(OAr_{2H}), and (d) five-coordinate $[(porphine)Ru(NO)]^+$. [B3P86/DGDZVP; visualized using iQmol]

It is evident from Figure 4a-c that the HOMOs are largely localized on the axial ON–Ru–aryloxide fragment, with a large contribution from the axial aryloxide ligand. In contrast, the HOMO of the five-coordinate $[(porphine)Ru(NO)]^+$ cation is localized

largely on the porphine macrocycle. These results led us to hypothesize that electrooxidation of the (OEP)Ru(NO)(OAr_{xH}) compounds should result in a net electron removal event that would most likely involve the axial aryloxide ligands. We sought to then perform preliminary electrochemistry experiments to test this hypothesis.

Electrochemistry

The redox behavior of the (por)Ru(NO)(OAr_{xH}) compounds were investigated via cyclic voltammetry (CV). Table 2 lists the formal potentials ($E°'$), peak anodic potentials (E_{pa}), peak potential separation (ΔE_p) and peak current ratios (i_{pc}/i_{pa}) of the first oxidations for these complexes. Perhaps not surprisingly, the compounds possessing more internal H bonds demonstrated the most positive oxidation potentials. Similar effects on redox potentials have been determined for the five-coordinate aryloxide (por)Fe(OArxH) [28-29] and thiolate (por)Fe(SArxH) [29-30] (por = TPP, OEP) complexes. In addition, effects of such internal H-bonds have been probed experimentally[31] and computationally[32] for the six-coordinate (porphine)Fe(NO)(SArxH) models. To determine whether the first oxidations were fully chemically reversible, i_{pc}/i_{pa} values were calculated, which confirmed that none of the compounds had a completely chemically reversible first oxidation at the scan rates employed. The compound closest to full chemical reversibility at 400 mV/s was the parent (OEP)Ru(NO)(OPh) with an i_{pc}/i_{pa} value of 0.88. Since the OAr_{2H} derivative displayed an irreversible first oxidation at all scan rates employed in our work, values for $E°'$, ΔE_p and i_{pc}/i_{pa} could not be determined.

Table 2. Redox potentials and peak current ratios for the first oxidations of (por)Ru(NO)(OAr_{xH}) (x = 0, 1, 2).[a]

	$E°'$	E_{pa}	ΔE_p	i_{pc}/i_{pa}
(OEP)Ru(NO)(OPh)	+0.43	+0.46	70 (60)	0.88
(OEP)Ru(NO)(OAr_{1H})	+0.52	+0.55	78 (58)	0.81
(OEP)Ru(NO)(OAr_{2H})	-	+0.58	-	-

[a] Experimental conditions: 1.0 mM analyte in CH_2Cl_2 containing 0.1 M NBu_4PF_6. Formal ($E°'$) and peak anodic (E_{pa}) potentials in V were measured with a Pt working electrode and referenced to $Fc^{0/+}$ and set to 0.00 V. ΔE_p values in parentheses (mV) refer to peak potential separation of $Fc^{0/+}$. Determined from voltammograms recorded at 400 mV/s.

The voltammogram of the OPh complex in CH_2Cl_2 with 0.1M NBu_4PF_6 as the supporting electrolyte is depicted in Figure 5. The full voltammogram within the solvent system limits were recorded at 200 mV/s with potentials referenced against the internal standard ferrocene ($Fc^{0/+}$) set to 0 V. No redox events were observed when scanning the reduction (negative) potentials up to –1.60 V vs $Fc^{0/+}$. Consequently, our electrochemical and spectroelectrochemical discussion will focus on the anodic processes. The 1-electron first oxidation of (OEP)Ru(NO)(OPh) at 100 mV/s was observed at a peak anodic potential (E_{pa}) of +0.46 V, which is similar to that determined previously for (OEP)Ru(NO)(OEt) at +0.44 V.[19] The first electrooxidation for (OEP)Ru(NO)(OPh) becomes increasingly chemically reversible when the switching potential (E_{sw}) is selected to isolate this initial feature (Figure 5, top) and upon increasing the scan rate to 400 mV/s (i_{pc}/i_{pa} = 0.88). This behavior is characteristic of an electrochemical transfer step involving a subsequent chemical change, or *EC* mechanism, which is likely a result of the aryloxide dissociation to generate a $[(OEP)Ru(NO)]^+$ product.

The OAr_{1H} complex exhibits generally similar redox behavior to the OPh derivative as observed in Figure 5 (Supporting Information Figure S5), and the slight decrease in chemical reversibility for the OAr_{1H} complex suggests the aryloxide dissociation is more prevalent compared to that of OPh when producing the $[(OEP)Ru(NO)]^+$ species. We find that the first oxidation of (OEP)Ru(NO)(OAr_{2H}) was chemically irreversible at the scan rates employed in this work (Supporting Information Figure S6). In any event, the cyclic voltammetry data suggested that the complexes were increasingly difficult to oxidize when more internal H-bonds were present.

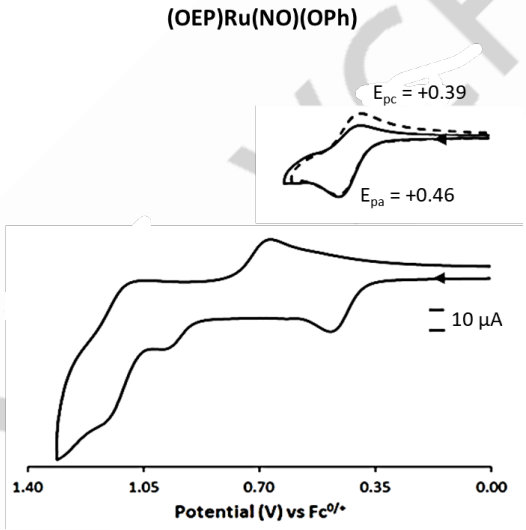

Figure 5. Cyclic voltammogram of 1.0 mM (OEP)Ru(NO)(OPh) in CH_2Cl_2 containing 0.1 M NBu_4PF_6 showing (top) first oxidation at scan rates of 100 mV/s (solid line) and 400 mV/s (dashed line) and (bottom) full voltammogram at a scan rate of 200 mV/s.

The cyclic voltammetry results for these (OEP)Ru(NO)(OArxH) compounds showing scan-rate dependence on chemical reversibility at these relatively low scan rates contrast with results from compounds such as the organometallic (T(*p*-OMe)PP)Ru(NO)Me that displays full reversibility at 200 mV.[33]

Infrared Spectroelectrochemistry

Preliminary IR spectroelectrochemistry was performed in order to probe the site(s) of oxidation for the electrochemical/chemical processes observed in the cyclic voltammograms in Figure 5. To obtain this information, difference IR spectra were recorded prior to and during the application of a predetermined potential, which was chosen to be sufficiently past the E_{pa} (~50 mV) for the first oxidation feature in the voltammogram. The difference IR spectrum of (OEP)Ru(NO)(OPh) in CH_2Cl_2 containing 0.1 M NBu_4PF_6 resulting from the first oxidation (Figure 6) reveals the consumption of the initial υ_{NO} at 1820 cm^{-1} and appearance of a new υ_{NO} at 1876 cm^{-1} ($\Delta\upsilon_{NO}$ = +56 cm^{-1}) after the analyte was held at a potential of +0.50 V vs the $Fc^{0/+}$ couple.

Figure 6. Difference IR spectrum showing the first oxidation products of (OEP)Ru(NO)(OPh) in CH_2Cl_2 containing 0.1 M NBu_4PF_6, with the potential held at +0.50 V vs $Fc^{0/+}$.

This $\Delta\upsilon_{NO}$ shift of +56 cm^{-1} upon oxidation of (OEP)Ru(NO)(OPh) is larger than the ~+20 cm^{-1} shifts observed after related electrooxidations of (T(*p*-OMe)PP)Ru(NO)(alkoxide) and –(carboxylate) complexes[18] that generate π-cation radicals where electron removal occurred at the porphyrin macrocycles.[34]

Appearance of the new υ_{NO} at 1876 cm^{-1} on the timescale of the spectroelectrochemical experiment suggests the formation of either $[(OEP)Ru(NO)(OPh)]^+$ or more likely a solvated $[(OEP)Ru(NO)(solv)]^+$ species that results from the eventual dissociation of the phenoxide ligand under longer timescale of the spectroelectrochemical experiment. We note that electrochemically generated $[(OEP)Ru(NO)(H_2O)]^+$ in CH_2Cl_2/Bu_4NClO_4 displays a υ_{NO} of 1877 cm^{-1}.[26] An additional but low intensity band at 1595 cm^{-1} during the first oxidation is also observed, which is in the range matching either the formation of an OEP-containing π-cation radical[34] or the presence of $\upsilon_{C=C}$ of a phenoxide radical;[35-36] the former would support an equatorial porphyrin centered oxidation, whereas the latter would support the notion of an initial ligand-centered oxidation consistent with our DFT calculations of the HOMO.

Conclusions

A new series of (OEP)Ru(NO)(OAr_{xH}) (x = 0, 1 and 2) derivatives have been prepared and characterized. The IR data reveals higher υ_{NO} frequencies in complexes with an increasing number of internal H-bonds. This shift is the result of a decrease in electron density at the oxygen atom through these internal hydrogen bonds leading to diminished π-backdonation to the Ru–NO fragment. The structural information of the OEP complexes exhibited longer Ru–O bond lengths with increasing intramolecular H-bonds. The anodic behavior of these complexes has shown that the redox potential for the first oxidation is increasingly positive with more intramolecular H-bonds present. A one-electron first oxidation and subsequent chemical process was observed that becomes more reversible at faster scan rates (> 200 mV/s) for the OPh and OAr_{1H} compounds, while the oxidations of the OAr_{2H} derivatives were chemically irreversible at all scan rates employed. The proposed successive chemical step was probed by IR spectroelectrochemistry which suggested an aryloxide ligand-centered oxidation and dissociation to generate what is likely a solvated $[(OEP)Ru(NO)]^+$ complex. These results provided a framework for a detailed mechanistic study of the electrochemical and spectroelectrochemical behavior of these and related tetraarylporphyrin (por)Ru(NO)(OArxH) complexes. These latter results will be detailed in a subsequent report.[37]

Experimental Section

General: All reactions were performed under an anaerobic (N_2) atmosphere using standard Schlenk glassware and/or in an Innovative Technology Labmaster 100 glove box. Solutions for spectral and electrochemical studies were also prepared under a nitrogen atmosphere. Dichloromethane, benzene and *n*-hexane were dried using an Innovative Technology Pure Solv 400-5-MD solvent purification system. 2-Trifluoroacetylaminophenol,[28] 2,6-bis(trifluoroacetylamino)phenol,[28] and (OEP)Ru(NO)(O-*i*-C_5H_{11}) (OEP = octaethylporphyrinato dianion)[15, 19-20] were synthesized as reported previously. Phenol (≥99%) was obtained from Aldrich and used as received. The supporting electrolyte NBu_4PF_6 (98%) obtained from Aldrich was recrystallized from hot ethanol and dried in vacuo. Ferrocene (98%) was obtained from Aldrich and sublimed prior to use. Chloroform-*d* ($CDCl_3$, 99.96% atom-D) was purchased from Cambridge Isotope Laboratories, deaerated and dried using activated 4 Å molecular sieves.

Instrumentation/Spectroscopy: Infrared spectra were recorded on a Bruker Tensor 27 FTIR spectrometer. ^1H spectra were obtained on a Varian 400 MHz spectrometer and the ^1H signals were referenced to the residual signal of the solvent employed ($CHCl_3$ at δ = 7.26 ppm). X-ray diffraction data was collected using a D8 Quest κ-geometry diffractometer with a Bruker Photon II cpad area detector and Mo-K_α source (λ = 0.71073 Å).

Computational details: Quantum mechanical electronic ground-state calculations were performed using the density functional theory (DFT) method.[38-39] The Gaussian09 software package was used, with iQmol as the visualization package. Molecular geometry optimization was carried out using the B3P86 functional and DGDZVP basis set.

Electrochemistry: Cyclic voltammetry measurements were obtained using a BAS CV 50W instrument. A three-electrode cell was utilized and consisted of a 3.0 mm diameter Pt disk working electrode, a Pt wire counter electrode and a Ag wire pseudo-reference electrode. Obtained products were dried under high vacuum for a minimum of 24 h prior to experiments. Solutions of the compounds were deaerated prior to use by passing a stream of N_2 gas through the solution for a minimum of 10 min, and a blanket of N_2 was maintained over the solution while performing the experiments. The solutions contained 1.0 mM of the analyte in 0.1 M NBu_4PF_6 as support electrolyte. Ferrocene (Fc, 1.0 mM) was used as an internal standard, and potentials were referenced to the $Fc^{0/+}$ couple set to 0.00 V. A Bruker Tensor 27 FTIR spectrometer, equipped with a mid-IR fiber-optic dip probe and liquid nitrogen cooled MCT detector (RemSpec Corporation, Sturbridge, MA, USA), was used for the IR spectroelectrochemistry.[19, 40-41]

(OEP)Ru(NO)(OPh): To a stirred CH_2Cl_2 (15 mL) solution of (OEP)Ru(NO)(O-*i*-C_5H_{11}) (40 mg, 0.053 mmol) was added phenol (10 mg, 0.11 mmol). The mixture was stirred for 4 h and the reaction progress was monitored by IR spectroscopy. A new band at 1825 cm^{-1} formed with concomitant and complete disappearance of the starting υ_{NO} band of (OEP)Ru(NO)(O-*i*-C_5H_{11}) at 1792 cm^{-1}. The solvent was removed in vacuo, and the residue re-dissolved in benzene and passed through an alumina column (Activity Grade III). Benzene was used to elute a dark red band that was collected. The solvent of this collected band was removed in vacuo and the product obtained in 72% yield (29 mg, 0.038 mmol). IR (KBr, cm^{-1}): υ_{NO} = 1823. ^1H NMR (400 MHz; $CDCl_3$): δ 10.28 (s, 4H, *meso*-H of OEP), 5.47 (t, 1H, *p*-H of

phenolate moiety, *J* = 8 Hz), 5.32 (t, 2H, *m*-H of phenolate moiety, *J* = 8 Hz), 4.16 (m, 16H, –C*H*$_2$CH$_3$ of OEP), 1.97 (t, 24H, –CH$_2$C*H*$_3$ of OEP, *J* = 8 Hz), 1.09 (d, 2H, *o*-H of phenolate moiety, *J* = 8 Hz). X-ray diffraction quality crystals were obtained by liquid/liquid diffusion in a sealed NMR tube using CH_2Cl_2 as the solvent and *n*-hexane as the antisolvent (1:1).

(OEP)Ru(NO)(OAr$_{1H}$): This compound was prepared similarly as above from (OEP)Ru(NO)(O-*i*-C_5H_{11}) (40 mg, 0.053 mmol) using 2-trifluoroacetylaminophenol (16 mg, 0.078 mmol). The chromatographed product was obtained in 76% yield (35 mg, 0.040 mmol). IR (KBr, cm^{-1}): υ_{NH} = 3336, υ_{NO} = 1830, υ_{CO} = 1718. ^{1}H NMR (400 MHz; $CDCl_3$): δ 10.34 (s, 4H, *meso*-H of OEP), 6.46 (d, 1H, *m*-H of phenolate moiety, *J* = 8 Hz), 5.50 (t, 1H, *p*-H of phenolate moiety, *J* = 8 Hz), 5.21 (t, 1H, *m*-H of phenolate moiety, *J* = 8 Hz), 4.15 (app m, 16H, –C*H*$_2$CH$_3$ of OEP), 2.77 (br s, 1H, NH of axial ligand), 1.97 (t, 24H, –CH$_2$C*H*$_3$ of OEP, *J* = 8 Hz), 0.44 (d, 1H, *o*-H of phenolate moiety, *J* = 8 Hz). X-ray diffraction quality crystals were obtained by slow evaporation from its CH_2Cl_2/cyclohexane (1:1) solution over a period of several days under a nitrogen atmosphere.

(OEP)Ru(NO)(OAr$_{2H}$): This compound was prepared similarly as above from (OEP)Ru(NO)(O-*i*-C_5H_{11}) (40 mg, 0.053 mmol) using 2,6-bis(trifluoroacetylamino)phenol (25 mg, 0.078 mmol). The chromatographed product was obtained in 61% yield (32 mg, 0.033 mmol). IR (KBr, cm^{-1}): υ_{NH} = 3367 and 3341, υ_{NO} = 1843, υ_{CO} = 1722. ^{1}H NMR (400 MHz; $CDCl_3$): δ 10.32 (s, 4H, *meso*-H of OEP), 6.48 (d, 2H, *m*-H of phenolate moiety, *J* = 8 Hz), 5.73 (t, 1H, *p*-H of phenolate moiety, *J* = 8 Hz), 4.18 (m, 16H, –C*H*$_2$CH$_3$ of OEP), 2.42 (br s, 2H, NH of axial ligand), 1.97 (t, 24H, –CH$_2$C*H*$_3$ of OEP, *J* = 8 Hz). X-ray diffraction quality crystals were obtained by slow evaporation from its CH_2Cl_2/cyclohexane (1:1) solution over a period of several days under a nitrogen atmosphere.

The three compounds above were also obtained when the reactions were performed in toluene and the products isolated by chromatography using silica and CH_2Cl_2.

CCDC 2005044 (for (OEP)Ru(NO)Ph), 2005005 (for (OEP)Ru(NO)(OAr$_{1H}$)), and 2005006 (for (OEP)Ru(NO)(OAr$_{2H}$)) contain the supplementary crystallographic data for this paper. These data can be obtained free of charge from The Cambridge Crystallographic Data Center.

Supporting Information

^{1}H NMR spectra, crystal and structure refinement data, DFT-calculated LUMO diagrams, and additional cyclic voltammograms.

Acknowledgements

This material is based upon work supported by (while GBR-A was serving at) the U.S. National Science Foundation (NSF; CHE-2154603 and CHE-1900181 to GBR-A and MJS). Any opinions, findings, and conclusions or recommendations expressed in this material are those of the authors and do not necessarily reflect the views of the NSF. We are grateful to Dr. Douglas R. Powell for the X-ray crystal structure determinations.

Keywords: porphyrinoids • nitrogen oxides • infrared spectroelectrochemistry • transition metals • cyclic voltammetry

References

[1] T. J. Reid III, M. R. N. Murthy, A. Sicignano, N. Tanaka, W. D. L. Musick, M. G. Rossman, *Proc. Natl. Acad. Sci. U. S. A.* **1981**, *78*, 4767-47771.
[2] T.-P. Ko, J. Day, A. J. Malkin, A. McPherson, *Acta Cryst. D* **1999**, *D55*, 1383-1394.
[3] T.-P. Ko, M. K. Safo, F. N. Musayev, M. L. Di Salvo, C. Wang, S.-H. Wu, D. L. Abraham, *Acta Cryst. D* **2000**, *D56*, 241-245.
[4] G. N. Murshudov, A. I. Grebenko, J. A. Brannigan, A. A. Antson, V. V. Barynin, G. G. Dodson, Z. Dauter, K. S. Wilson, W. R. Melik-Adamyan, *Acta Cryst. D* **2002**, *58*, 1972-1982.
[5] M. J. Mate, G. Murshudov, J. Bravo, W. Melik-Adamyan, P. C. Loewen, I. Fita, in *Handbook of Metalloproteins, Vol. 1* (Eds.: A. Messerschmidt, R. Huber, K. Wieghardt, T. Poulos), John Wiley and Sons, New York, **2001**, pp. 486-502.
[6] J.-H. Jeoung, D. A. Pippig, B. M. Martins, N. Wagener, H. Dobbekn, *J. Mol. Biol.* **2007**, *368*, 112-1131.
[7] M. L. Oldham, A. R. Brash, M. E. Newcomer, *Proc. Natl. Acad. Sci. U. S. A.* **2004**, *102*, 297-302.
[8] J. Geng, K. Dornevil, V. L. Davidson, A. Liu, *Proc. Natl. Acad. Sci. U. S. A.* **2013**, *110*, 9639-9644.
[9] C. F. M. Gaudin, J. C. Grigg, A. L. Arrieta, M. E. P. Murphy, *Biochemistry* **2011**, *50*, 5443-5452.
[10] N. Lehnert, E. Kim, H. T. Dong, J. B. Harland, A. P. Hunt, E. C. Manickas, K. M. Oakley, J. Pham, G. C. Reed, V. S. Alfaro, *Chem. Rev.* **2021**, *121*, 14682-14905.
[11] L. Cheng, G. B. Richter-Addo, in *The Porphyrin Handbook, Vol. 4 (Biochemistry and Binding: Activation of Small Molecules)* (Eds.: R. Guilard, K. Smith, K. M. Kadish), Academic Press, New York, **2000**, pp. 219-291.
[12] J. R. Zink, E. G. Abucayon, A. R. Ramuglia, A. Fadamin, J. E. Eilers, G. B. Richter-Addo, M. J. Shaw, *ChemElectroChem* **2018**, *5*, 861-871.
[13] E. G. Abucayon, D. R. Powell, G. B. Richter-Addo, *J. Am. Chem. Soc.* **2017**, *139*, 9495-9498.
[14] G.-B. Yi, M. A. Khan, D. R. Powell, G. B. Richter-Addo, *Inorg. Chem.* **1998**, *37*, 208-214.
[15] J. Lee, G.-B. Yi, M. A. Khan, G. B. Richter-Addo, *Inorg. Chem.* **1999**, *38*, 4578-4584.
[16] J. Lee, B. Twamley, G. B. Richter-Addo, *Dalton Trans.* **2004**, 189-196.
[17] G.-B. Yi, M. A. Khan, G. B. Richter-Addo, *Inorg. Chem.* **1996**, *35*, 3453-3454.
[18] D. Awasabisah, N. Xu, K. P. S. Gautam, D. R. Powell, M. J. Shaw, G. B. Richter-Addo, *Eur. J. Inorg. Chem.* **2016**, *19*, 509-518.
[19] S. M. Carter, J. Lee, C. A. Hixson, D. R. Powell, R. A. Wheeler, M. J. Shaw, G. B. Richter-Addo, *Dalton Trans.* **2006**, 1338-1346.
[20] D. V. Fomitchev, P. Coppens, T. Li, K. A. Bagley, L. Chen, G. B. Richter-Addo, *Chem. Commun.* **1999**, 2013-2014.
[21] G.-B. Yi, M. A. Khan, G. B. Richter-Addo, *Chem. Commun.* **1996**, 2045-2046.
[22] G.-B. Yi, L. Chen, M. A. Khan, G. B. Richter-Addo, *Inorg. Chem.* **1997**, *36*, 3876-3885.
[23] D. S. Bohle, P. A. Goodson, B. D. Smith, *Polyhedron* **1996**, *15*, 3147-3150.
[24] A. Antipas, J. W. Buchler, M. Gouterman, P. D. Smith, *J. Am. Chem. Soc.* **1978**, *100*, 3015-3024.
[25] D. S. Bohle, C.-H. Hung, B. D. Smith, *Inorg. Chem.* **1998**, *37*, 5798-5806.
[26] P. Singh, A. K. Das, B. Sarkar, M. Niemeyer, F. Roncaroli, J. A. Olabe, J. Fiedler, S. Zalis, W. Kaim, *Inorg. Chem.* **2008**, *47*, 7106-7113.
[27] N. Xu, J. Lee, D. R. Powell, G. B. Richter-Addo, *Inorg. Chim. Acta* **2005**, *358*, 2855-2860.
[28] D. Kanamori, Y. Yamada, A. Onoda, T.-A. Okamura, S. Adachi, H. Yamamoto, N. Ueyama, *Inorg. Chim. Acta* **2005**, *358*, 331-338.
[29] N. Ueyama, N. Nishikawa, Y. Yamada, T.-a. Okamura, A. Nakamura, *Inorg. Chim. Acta* **1998**, *283*, 91-97.
[30] N. Ueyama, N. Nishikawa, Y. Yamada, T.-A. Okamura, S. Oka, H. Sakurai, A. Nakamura, *Inorg. Chem.* **1998**, *37*, 2415-2421.
[31] N. Xu, D. R. Powell, L. Cheng, G. B. Richter-Addo, *Chem. Commun.* **2006**, 2030-2032.
[32] F. Paulat, N. Lehnert, *Inorg. Chem.* **2007**, *46*, 1547-1549.
[33] N. Xu, J. Lilly, D. R. Powell, G. B. Richter-Addo, *Organometallics* **2012**, *31*, 827-834.
[34] E. T. Shimomura, M. A. Phillippi, H. M. Goff, W. F. Scholz, C. A. Reed, *J. Am. Chem. Soc.* **1981**, *103*, 6778-6780.

[35] J. Spanget-Larsen, M. Gil, A. Gorski, D. M. Blake, J. Waluk, J. G. Radziszewski, *J. Am. Chem. Soc.* **2001**, *123*, 11253-11261.
[36] R. Schnepf, A. Sokolowski, J. Muller, V. Bachler, K. Wieghart, P. Hildebrandt, *J. Am. Chem. Soc.* **1998**, *120*, 2352-2364.
[37] A. R. Ramuglia, J. R. Zink, A. J. Warhausen, E. G. Abucayon, N. Xu, K. Shrestha, G. B. Richter-Addo, M. J. Shaw, *Submitted* **2024**.
[38] R. G. Parr, W. Yang, *Density-Functional Theory of Atoms and Molecules*, Oxford University Press, New York, **1989**.
[39] A. D. Becke, *J. Chem. Phys.* **2014**, *140*, 18A301.
[40] M. J. Shaw, R. L. Henson, S. E. Houk, J. W. Westhoff, M. W. Jones, G. B. Richter-Addo, *J. Electroanal. Chem.* **2002**, *534*, 47-53.
[41] Z. N. Zahran, M. J. Shaw, M. A. Khan, G. B. Richter-Addo, *Inorg. Chem.* **2006**, *45*, 2661-2668.

Entry for the Table of Contents

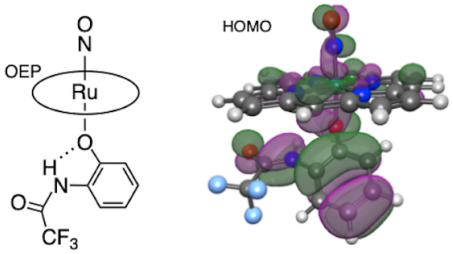

Ruthenium nitrosyl porphyrins with *trans* aryloxides that differ in the number of internal H-bonds have been prepared. Cyclic voltammetry of these (OEP)Ru(NO)(OArxH) (OEP = octaethylporphyrinato dianion) compounds reveal electrooxidations with variable chemical reversibility that correlate with the number of internal H-bonds. DFT-calculated HOMOs suggest electron removal resulting in the net loss of the *trans* aryloxides.

Supporting Information

Ruthenium nitrosyl porphyrins coordinated with aryloxides containing internal hydrogen bonds

Adam J. Warhausen, Jeremy R. Zink, Bradley J. Ross, Anthony R. Ramuglia, Jennifer Londoño-Salazar, Michael J. Shaw, and George B. Richter-Addo

Table of Contents

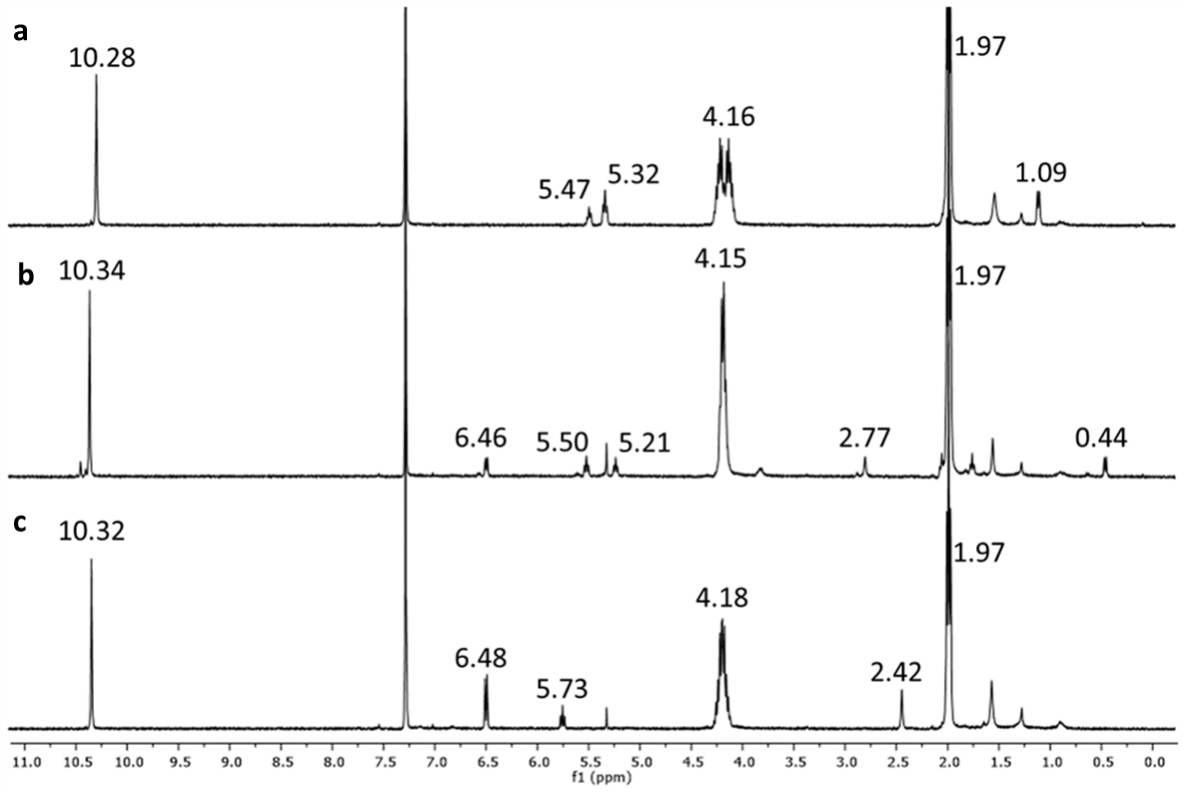

Figure S1. Stacked ^{1}H NMR spectra of (a) (OEP)Ru(NO)(OPh), (b) (OEP)Ru(NO)(OAr_{1H}), and (c) (OEP)Ru(NO)(OAr_{2H}) in $CDCl_3$ with characteristic chemical shifts of porphyrin and phenolate proton signals reported. Minor impurity peaks due to CH_2Cl_2 (5.31 ppm), H_2O (1.59 ppm) and *n*-hexane (0.88 ppm and 1.25 ppm) are also present.

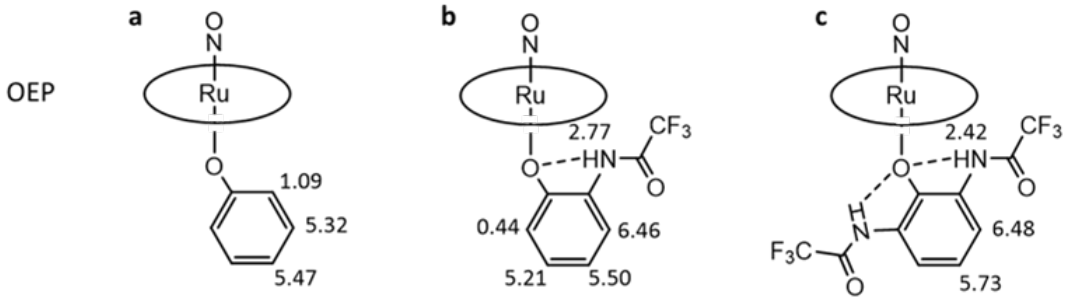

Figure S2. Assigned ^{1}H NMR chemical shifts (ppm) of the axial aryloxide ligands in (a) (OEP)Ru(NO)(OPh), (b) (OEP)Ru(NO)(OAr_{1H}), and (c) (OEP)Ru(NO)(OAr_{2H}).

Table S1. Crystal and structure refinement data.

Compound	(OEP)Ru(NO)(OPh)	(OEP)Ru(NO)(OAr_{1H})	(OEP)Ru(NO)(OAr_{2H})
CCDC	2005044	2005005	2005006
Empirical Formula	$C_{42}H_{49}N_5O_2Ru$	$2(C_{44}H_{49}F_3N_6O_3Ru)\bullet(C_8H_6F_3N_1O_2)\bullet(C_6H_{12})$	$C_{46}H_{49}F_6N_7O_4Ru$
Formula weight	756.93	2025.21	978.99
Crystal system	Monoclinic	Monoclinic	Orthorhombic
Temperature	100(2) K	100(2) K	100(2) K
Space group	$P2_1/c$	$P2_1/c$	$Pbca$
a (Å), α(°)	12.9498(10), 90	15.140(2), 90	17.6424(19), 90
b (Å), β(°)	37.165(4), 104.058(4)	21.887(3), 103.966(2)	19.177(2), 90
c (Å), γ(°)	7.8320(7), 90	14.7336(19), 90	26.409(3), 90
V, Z/Z'	3656.5(6) $Å^3$, 4/1	4737.9(11) $Å^3$, 2/0.5	8934.9(17) $Å^3$, 8/1
D(calcd), g/cm^3	1.375	1.420	1.456
Abs coeff, mm^{-1}	0.472	0.401	0.428
F(000)	1584	2104	4032
θ range for data collection	2.192–28.282°	1.386–28.394°	1.542–21.036°
Reflections collected	68111	59598	63323
Independent reflns	9070 [R_{int} = 0.1426]	11838 [R_{int} = 0.0642]	4821 [R_{int} = 0.1120]
Data / restraints / parameters	9070 / 0 / 451	11838 / 438 / 752	4821 / 71 / 596
Goodness-of-fit on F^2	1.000	1.000	1.018
Observed data [$I>2\sigma(I)$]	6112	9073	3753
Final R indices [$I>2\ \sigma(I)$]	R1 = 0.0774	R1 = 0.0469	R1 = 0.0459
R indices (all data)	wR2 = 0.2140	wR2 = 0.1164	wR2 = 0.1135
Largest diff. peak and hole, e.$Å^{-3}$	1.930 and –1.829	1.102 and –0.446	0.488 and –0.473

$wR2 = \{\Sigma[w(F_o^2 - F_c^2)^2] / \Sigma\ [w(F_o^2)^2]\}^{1/2}$

$R1 = \Sigma\ ||F_o| - |F_c|| / \Sigma\ |F_o|$

(a)

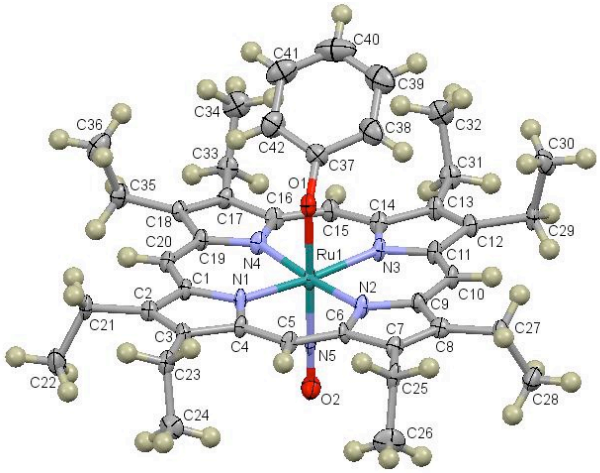

(b)

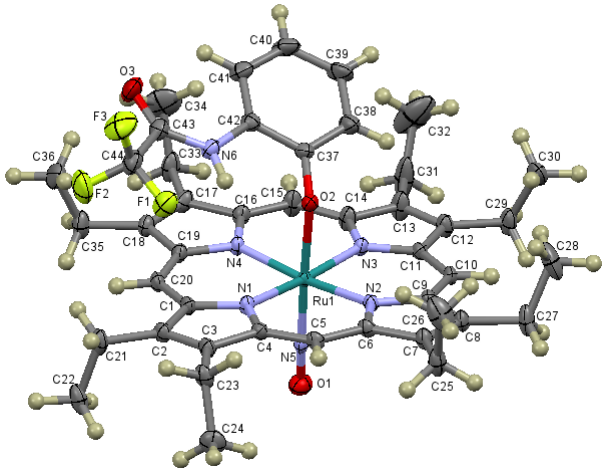

(c)

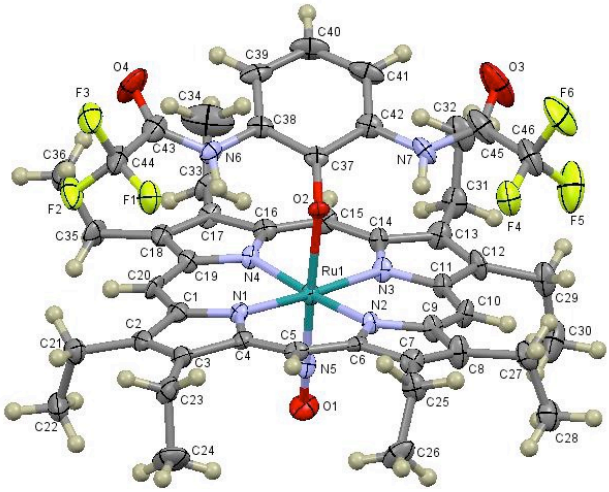

Figure S3. Thermal ellipsoid plots and atom labelling for (a) (OEP)Ru(NO)(OPh), (b) (OEP)Ru(NO)(OAr_{1H}) [The H-atom bonded to N6 was located on a difference map and was refined independently], and (c) (OEP)Ru(NO)(OAr_{2H}).

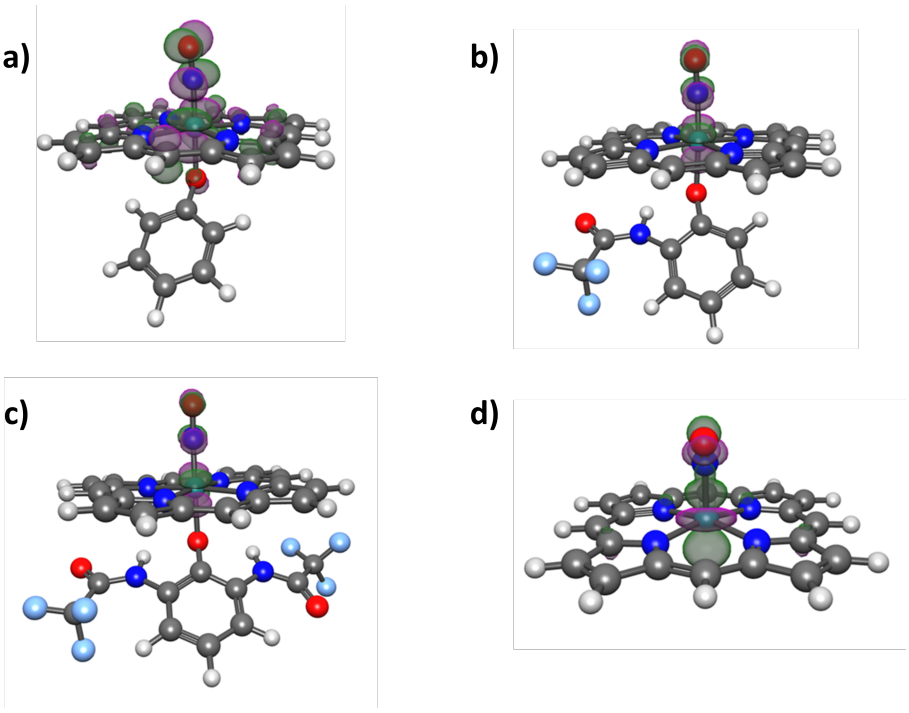

Figure S4. DFT calculated LUMOs for the model (a) (porphine)Ru(NO)(OPh), (b) (porphine)Ru(NO)(OAr_{1H}), (c) (porphine)Ru(NO)(OAr_{2H}), and (d) five-coordinate [(porphine)Ru(NO)]$^{+}$ complexes.

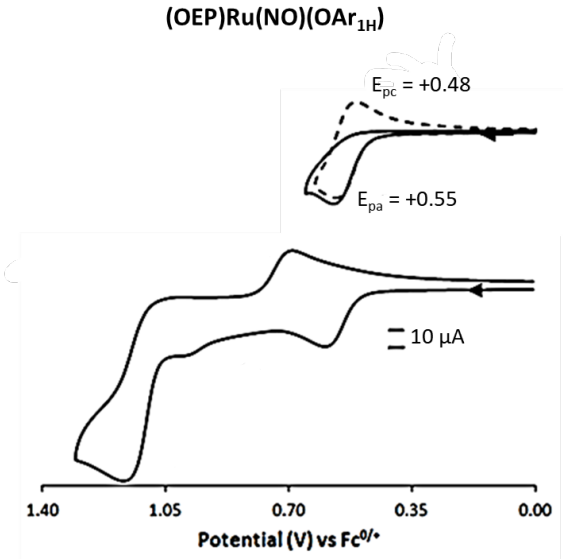

Figure S5. Cyclic voltammogram of 1.0 mM (OEP)Ru(NO)(OAr_{1H}) in CH_2Cl_2 containing 0.1 M NBu_4PF_6 showing (top) first oxidation at scan rates of 100 mV/s (solid line) and 400 mV/s (dashed line) and (bottom) full voltammogram at a scan rate of 200 mV/s.

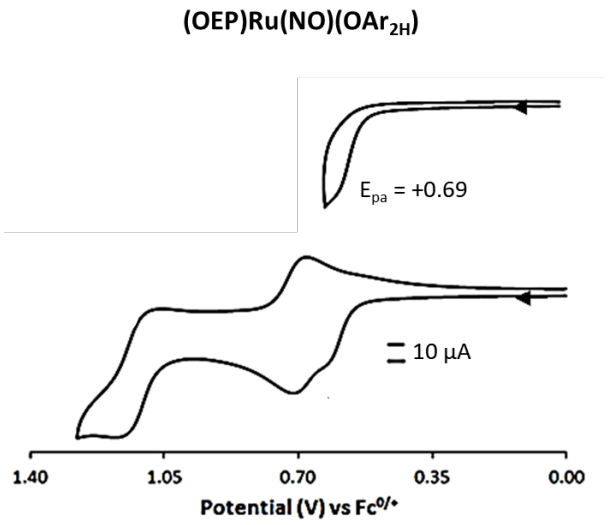

Figure S6. Cyclic voltammogram of 1.0 mM (OEP)Ru(NO)(OAr_{2H}) in CH_2Cl_2 containing 0.1 M NBu_4PF_6 showing (top) first oxidation and (bottom) full voltammogram at a scan rate of 200 mV/s.